

This document is confidential and is proprietary to the American Chemical Society and its authors. Do not copy or disclose without written permission. If you have received this item in error, notify the sender and delete all copies.

Separation of Halogen Atoms by Sodium from Dehalogenative Reactions on a Au(111) Surface

Journal:	<i>ACS Nano</i>
Manuscript ID	nn-2023-129498.R2
Manuscript Type:	Article
Date Submitted by the Author:	27-Feb-2024
Complete List of Authors:	Zhang, Zhaoyu; Tongji University Gao, Yuhong; Tongji University, Interdisciplinary Materials Research Center, Tongji-Aarhus Joint Research Center for Nanostructures and Functional Nanomaterials, College of Materials Science and Engineering Yi, Zewei; Tongji University Zhang, Chi; Tongji University, School of Materials Science and Engineering Xu, Wei; Tongji University, Interdisciplinary Materials Research Center, Tongji-Aarhus Joint Research Center for Nanostructures and Functional Nanomaterials, College of Materials Science and Engineering

SCHOLARONE™
Manuscripts

Separation of Halogen Atoms by Sodium from Dehalogenative Reactions on a Au(111) Surface

Zhaoyu Zhang, Yuhong Gao, Zewei Yi, Chi Zhang,* Wei Xu*

Interdisciplinary Materials Research Center, School of Materials Science and Engineering,
Tongji University, Shanghai 201804, People's Republic of China.

*Corresponding author.

Email: Chi Zhang: zhangchi11@tongji.edu.cn; Wei Xu: xuwei@tongji.edu.cn

ABSTRACT On-surface dehalogenative reaction has been promising in the construction of nanostructures with diverse morphologies and intriguing electronic properties, while halogen (X), as the main byproduct, often impedes the formation of extended nanostructures and property characterization, and the reaction usually requires high C–X activation temperatures, especially on relatively inert Au(111). Enormous efforts in precursor design, halogen-to-halide conversion, and introduction of extrinsic metal atoms have been devoted to either eliminating dissociated halogens or reducing reaction barriers. However, it is still challenging to separate halogens from molecular systems while facilitating C–X activation under mild conditions. Herein, a versatile halogen separation strategy has been developed based on the introduction of extrinsic sodium (Na) into dehalogenative reactions on Au(111) as model systems that both isolates the dissociated halogens

1
2
3
4
5
6 and facilitates the C–Br activation under mild conditions. Moreover, the combination of scanning
7
8 tunneling microscopy imaging and density functional theory calculations reveals the formation of
9
10 sodium halides (NaX) from halogens in these separation processes, as well as the reduction in
11
12 reaction temperatures and barriers, demonstrating the versatility of extrinsic sodium as an effective
13
14 “cleaner” and “dehalogenator” of surface halogens. Our study demonstrates a valuable strategy to
15
16 facilitate the on-surface dehalogenative reactions, which will assist in the precise fabrication of
17
18 low-dimensional carbon nanostructures.
19
20

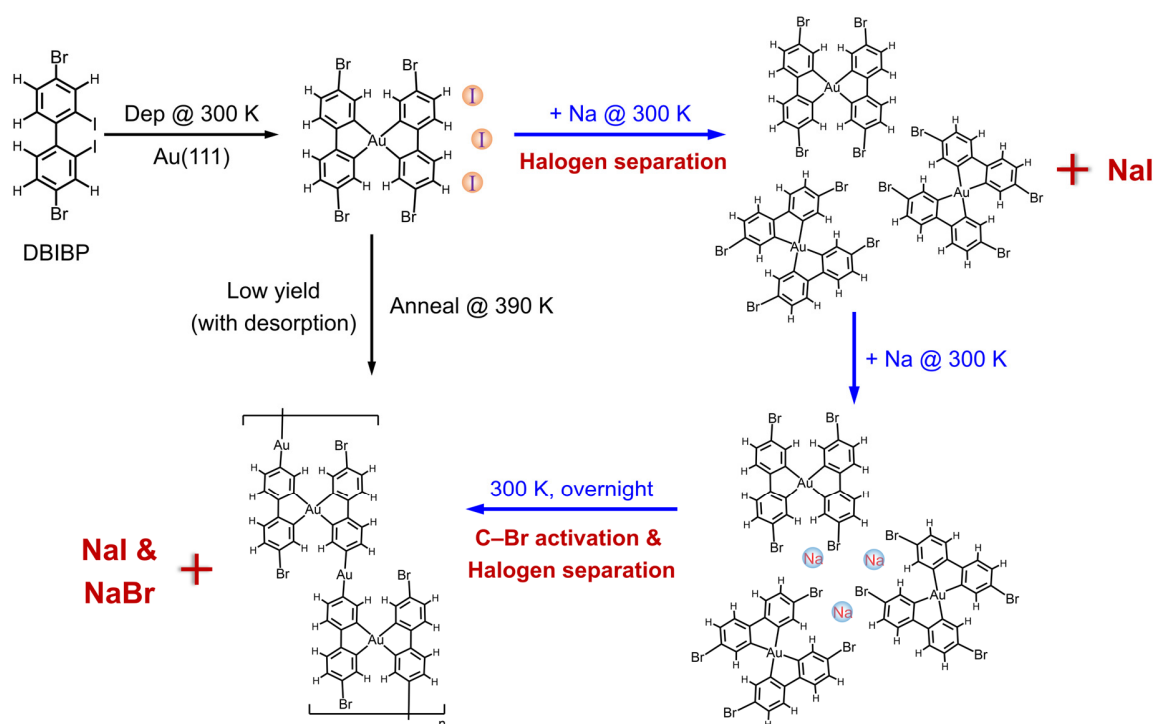
21
22
23 **KEYWORDS:** on-surface synthesis, C–Br activation, dehalogenative reaction, scanning tunneling
24
25 microscopy, density functional theory
26
27
28
29

30
31 On-surface synthesis has shown great promise in fabricating low-dimensional nanostructures
32
33 with atomic precision for potential molecule-based electronics, such as graphene nanoribbons and
34
35 other carbon-based nanostructures.¹⁻⁵ Among various on-surface reactions, Ullmann-type
36
37 dehalogenative coupling reaction, as the most widely used one, has successfully constructed
38
39 carbon nanostructures with diverse morphologies and intriguing electronic properties.⁶⁻⁸ Despite
40
41 the pre-designed and well-controlled reaction manner, dehalogenative coupling reactions suffer
42
43 from surrounding halogen obstacles, prohibiting the construction of extended carbon
44
45 nanostructures and the property characterization,⁹⁻¹¹ as well as high activation temperatures
46
47 accompanied by the desorption of precursors especially on inert Au(111). Accordingly, enormous
48
49 efforts have been devoted to the elimination of dissociated halogens and the reduction of reaction
50
51 barriers. Precursors with larger molecular weight were applied to avoid desorption, and samples
52
53 were generally annealed at high temperatures to reduce halogens.¹⁰⁻¹² Moreover, converting
54
55
56
57
58
59
60

1
2
3
4
5
6 halogens to halides with low adsorption energy is another strategy. Specifically, H₂ and Si have
7
8 been proved to be effective surface dehalogenators to form HBr and SiBr₄ from Br, respectively,
9
10 followed by desorption,¹³⁻¹⁵ which, yet, requires harsh reaction conditions (typically high pressure,
11
12 i.e., in the range of 10⁻⁷ mbar, and high substrate temperatures)^{15, 16} with possible quenching of
13
14 reactive radicals in the former case and produces 1,4-disilabenzene (C₄Si₂) linkers (embedded in
15
16 the molecular structures) in the latter.¹⁷ On the other hand, the introduction of extrinsic metal atoms,
17
18 e.g., Cu,¹⁸ Pd,¹⁹ Ni,²⁰ Dy,²¹ is an intriguing catalytic approach to lower the reaction temperatures
19
20 of C–Br activation, with dissociated halogens still remaining and metal atoms strongly embedded
21
22 in the organometallic structures. However, it remains a great challenge to eliminate the negative
23
24 impacts of halogens while facilitating C–Br activation under mild conditions. Therefore, it is of
25
26 general interest to develop an alternative strategy to both activate the C–Br bonds and isolate the
27
28 dissociated halogens from target carbon-based nanostructures, which should be significant for the
29
30 structure construction with atomic precision and accurate property characterization.
31
32
33
34
35

36 In this study, a halogen separation strategy is developed by introducing extrinsic sodium (Na)
37
38 into dehalogenative reactions on a Au(111) surface, which not only isolates the intermolecular
39
40 dissociated halogens, but also facilitates the intramolecular C–Br activation under mild conditions.
41
42 As a model system, 4,4'-dibromo-2,2'-diiodo-1,1'-biphenyl (DBIBP), containing both Br and I
43
44 substituents, was selected as the molecular precursor (Scheme 1). By a combination of high-
45
46 resolution scanning tunneling microscopy (STM) imaging and density functional theory (DFT)
47
48 calculations, Na-induced halogen separation processes on Au(111) have been visualized and
49
50 evidenced to lead to the progressive structural transformation and subsequent construction of Na-
51
52 interlinked intermediate structures, followed by further formation of coupled structures via C–Br
53
54 activation at room temperature (RT, ~300 K), which were also accompanied by the formation of
55
56
57
58
59
60

NaX (X: halogen) islands (Scheme 1). In addition, the universality of this separation strategy was also validated in both aspects, using a more general molecule, 4,4''-dibromo-1,1':4',1''-terphenyl (DBTP). Furthermore, DFT calculations reveal that the reaction barriers for C–Br activation are generally reduced in the presence of Na, and more importantly, the combination of Na with halogens (forming NaX) separates dissociated halogens from the corresponding reaction systems, resulting in the energetically more favorable situations compared to the Na-free cases. This study provides an effective strategy to steer the programmable dehalogenative reactions, which should benefit the construction of low-dimensional carbon-based nanostructures.



Scheme 1. Schematic illustration showing the comparison between the Na-facilitated halogen separation strategy demonstrated in this study and the conventional Na-free dehalogenative reaction (indicated by blue and black arrows, respectively).

Results and discussion

1
2
3
4
5
6 After deposition of the DBIBP molecule on Au(111) held at ~300 K, large islands composed of
7
8 H-shaped motifs (shortened as H-motifs) formed (Figure 1a). The close-up STM image (Figure
9
10 1b) shows that H-motifs (as depicted by white contours) are densely aligned in a row surrounded
11
12 by inter-row bright dots (indicated by blue circles), which further expand into molecular islands.
13
14 In addition, each H-motif is composed of two bent rods as “legs” connected by a large bright dot
15
16 at the center, and each end of the legs is decorated with a dot. Based on the submolecularly resolved
17
18 STM image, an organometallic dimer structure²² with a Au adatom linking two molecular
19
20 components via C–Au contacts was calculated. The DFT-optimized structural model (left and
21
22 bottom panels of Figure 1c) shows that two DBIBP molecules are connected via a Au adatom
23
24 located in the bay region by forming four C–Au contacts as a result of deiodination^{23,24}, while four
25
26 Br substituents remain in the termini, in good agreement with the hierarchical dehalogenation
27
28 scenario as reported²⁵⁻²⁷. Accordingly, the STM simulation (right panel) successfully reproduces
29
30 the experimental topography. The small bright dots around the H-motifs are thus assigned to the
31
32 dissociated iodine atoms. In this way, the deiodination took place with the formation of H-motifs
33
34 and generation of free intermolecular halogens, which provides a model system to verify the
35
36 feasibility of introducing Na to separate halogens.
37
38
39
40
41
42
43
44
45
46
47
48
49
50
51
52
53
54
55
56
57
58
59
60

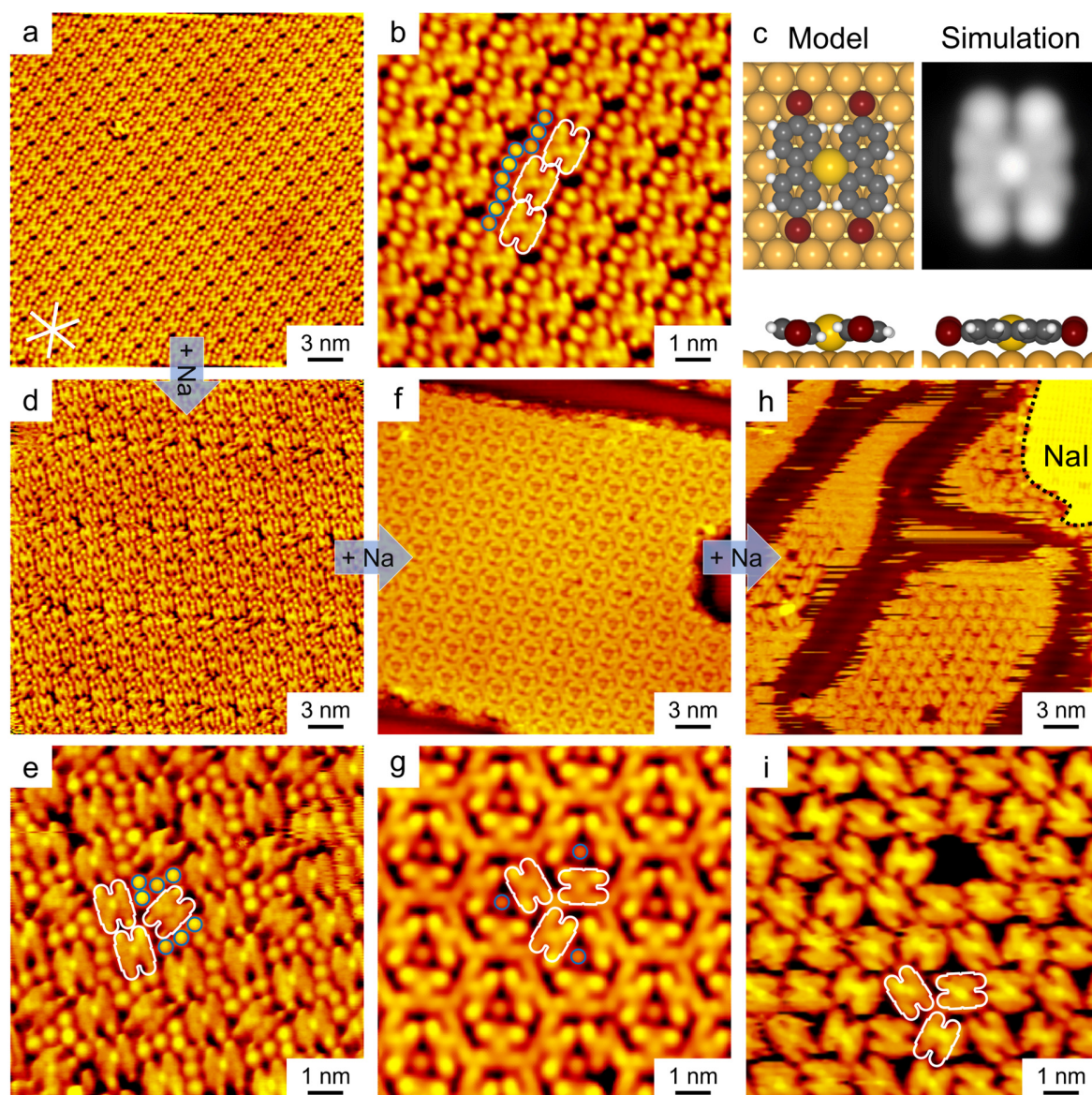


Figure 1. Gradual iodine separation from self-assembled molecular structures induced by Na on Au(111) at ~300 K. (a, d, f, h) Large-scale and (b, e, g, i) close-up STM images showing the gradual structural transformation with reduced adjacent iodine atoms, induced by progressive deposition of Na at ~300 K. The individual H-shaped motifs and iodine atoms are depicted by the white contours and blue circles, respectively. (c) Top and two side views of the DFT-calculated structural model and corresponding STM simulation (top right) of the H-motif. C: gray; H: white; Br: brown; Au: yellow. Scanning conditions: $V = -1.2$ V, and $I = 0.7$ nA. The close-packed

1
2
3
4
5
6 directions are illustrated as white lines in (a). The boundary of the NaI island is highlighted in
7
8 black dotted lines in (h). The STM images were recorded in a typical temperature range of 100 –
9
10 150 K.

11
12
13 Subsequently, pure Na atoms were dosed to the above sample held at ~300 K, leading to an obvious
14
15 phase transition (Figure 1d). From the close-up STM image (Figure 1e), individual H-motifs with
16
17 decreased surrounding halogens could be clearly identified. By providing more Na (see Methods
18
19 for more details) to the above sample in a controlled manner, further phase transition with
20
21 decreasing halogens occurred (Figure 1f), where the stoichiometric ratio of halogens/H-motifs
22
23 varied from ~3:1 (Figure 1a, b), through ~13:6 (Figure 1d, e), to ~1:3 (Figure 1f, g). The zoomed-
24
25 in STM image (Figure 1g) shows that three highlighted neighboring H-motifs form a chiral triangle
26
27 mainly via halogen bonds^{28, 29}, surrounded by three halogens at hydrogen-rich sites^{30, 31}.
28
29 Interestingly, after successive deposition of Na atoms, the remaining halogens were thoroughly
30
31 isolated from the molecular structures (Figure 1h, i), and small patches of H-motifs formed with
32
33 molecules in a fuzzy state under scanning conditions due to the absence of intermolecular
34
35 stabilizing halogens and the formation of weak intermolecular interactions (halogen bonds and C–
36
37 H···Br interactions)³² within H-motifs (Figure S1). Notably, during the introduction of Na atoms,
38
39 the transformation of the assembled structures of H-motifs was accompanied by this gradual
40
41 decreasing process of halogens until their complete isolation to form NaI salt islands (as shown in
42
43 Figure 1h and detailed in Figure S2), revealing that the strong electrostatic interactions between
44
45 Na and halogen atoms (i.e., I in this case) was the driving force for the successful isolation of
46
47 halogens from molecular structures and thus the molecular structural evolution³³. Hence, the
48
49 gradual intermolecular halogen isolation was realized by Na addition, leading to the separation of
50
51 released halogens from molecular structures.
52
53
54
55
56
57
58
59
60

1
2
3
4
5
6 It is known that halogens are able to stabilize molecular structures via electrostatic interactions,
7
8 as also shown above, but are generally obstacles to further coupling processes.^{11, 34} Inspired by our
9
10 recent studies^{33, 35, 36} and previous reports on extrinsic metal atoms¹⁸⁻²¹, additional Na atoms were
11
12 introduced into the above sample to test the possibility of promoting the dehalogenative reactions.
13
14 Upon further deposition of Na at ~300 K, a two-dimensional (2D) honeycomb network structure
15
16 was obtained (Figure 2a). From the close-up STM image, more details of the structure could be
17
18 recognized (Figure 2b), where each side of the six-membered rings consists of an H-motif with
19
20 less uniform bright junctions, which are presumably caused by the involvement of Na. In addition,
21
22 the relative positions of three H-motifs in the Na-interlinked metal-organic clusters are not exactly
23
24 the same, indicating different interaction modes between Na atoms and H-motifs. Based on the
25
26 typical features and previous reports^{37, 38}, the involvement of excess Na in the assembled structure
27
28 was proposed, and the corresponding DFT calculations on the structural models and STM
29
30 simulations were performed (Figure S3). Accordingly, these bright dots at the junctions could be
31
32 attributed to three, four or even more Na atoms³⁵ interacting with Br substituents of H-motifs in
33
34 different interaction modes. The model of a typical H₃Na₃ motif is shown in Figure 2c, in which
35
36 each Na interacts with three Br substituents via electrostatic interactions. The corresponding
37
38 network structure was thus tentatively superimposed on the zoomed-in STM image (Figure 2b),
39
40 showing a good agreement with the local part of the network. Moreover, the electrostatic potential
41
42 map of the typical H₃Na₃ motif (Figure 2d) shows that the Na atoms are positively charged, while
43
44 negative potential regions exist around the C–Br bond axes, which rationalizes the electrostatic
45
46 interactions between Na atoms and the surrounding Br substituents at the side position and accords
47
48 well with the recent report regarding the interaction between K and three Cl substituents.³⁷
49
50
51
52
53
54
55
56
57
58
59
60

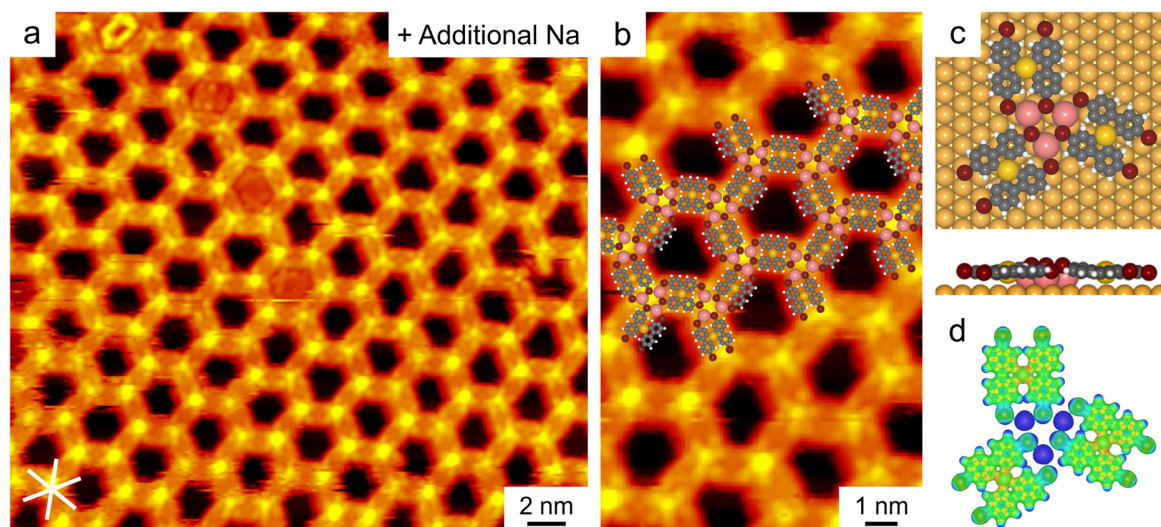


Figure 2. Construction of Na-interlinked metal-organic intermediate nanostructure by dosing additional Na at ~300 K. (a) Large-scale STM image of 2D honeycomb metal-organic nanostructure. (b) Close-up STM image partially superimposed with the DFT-optimized molecular network. Scanning conditions: $V = -1.2$ V, and $I = 0.7$ nA. The STM images were recorded in a typical temperature range of 100 – 150 K. (c) Top and side views of the DFT-calculated model of a Na-interlinked H₃Na₃ motif on Au(111). C: gray; H: white; Br: brown; Na: pink; Au: yellow. (d) Electrostatic potential map of the H₃Na₃ motif (the substrate was omitted for clarity), where blue and red colors represent positive and negative potential regions, respectively. The close-packed directions are indicated in (a).

After the construction of the Na-interlinked metal-organic nanostructure, such a sample was then kept at ~300 K for approximately 10 hours. Interestingly, islands of a well-ordered, densely packed nanostructure appeared with no more bright junctions inside, as shown in the large-scale STM image (Figure 3a), indicating an apparent phase transition. The submolecularly resolved STM image (Figure 3b) displays that the nanostructure is composed of dimers, i.e., the connection of two H-motifs, as indicated by the white contours. Such dimers of the same chirality are aligned in

1
2
3
4
5
6 one row, with those of the opposite chirality in the adjacent row, forming islands in an alternating
7
8 arrangement. A closer inspection reveals that two H-motifs are linked together by sharing one dot
9
10 at the joint, which could be attributed to the dissociation of two terminal Br atoms and the addition
11
12 of a Au adatom.³⁹ Then, DFT calculations on the dimer structure and the corresponding STM
13
14 simulation were performed (Figure 3c, d), which successfully reproduced the typical STM
15
16 morphology. In addition, the distance of the C–Au–C bond was measured to be $\sim 3.7 \pm 0.2$ Å from
17
18 the STM image (Figure S4), which is comparable to that obtained in both the DFT calculations
19
20 (4.1 Å) and the previous report (3–4 Å)³⁹, and is too long to be a covalent C–C bond. It is worth
21
22 noting that free Au adatoms are usually not involved in the organometallic intermediates in the
23
24 Ullmann-type coupling reactions on Au(111), but are embedded herein⁴⁰, which is probably due
25
26 to the steric hindrance caused by the staggered adsorption configuration of such an H-motif (see
27
28 the side view in Figure 1c), similar to the previous reports.^{39, 41} Moreover, the Au adatom located
29
30 at the junction of two H-motifs appears to be darker than those at the center of the H-motif (Figure
31
32 3b), suggesting stronger bonding of the bay-region C_{aryl}–metal in a tetra-bonding mode than that
33
34 of a single C_{aryl}–metal–C_{aryl} one. Meanwhile, the termini of the other joint sides are lifted away
35
36 from the surface (Figure S5), generally resulting in lower activity,⁴² which rationalizes the
37
38 dominance of the single-sided coupling. Therefore, with the assistance of excess Na, the C–Br
39
40 activation was validated to be feasible at RT.
41
42
43
44
45

46 Upon deposition of additional Na, these large well-ordered assembled islands (Figure 3a) were
47
48 found to further break up into small molecular islands, and isolated salt islands (labeled NaI +
49
50 NaBr) could also be clearly distinguished from these molecular islands (Figure 3e). The typical
51
52 close-up STM image (Figure 3f) provides more details that the molecular islands are composed of
53
54 organometallic oligomers with the NaX island isolated (where I and Br atoms appear as protrusions
55
56
57
58
59
60

of different brightness). Further magnified STM image (Figure 3g) shows that H-based oligomers (as typically indicated by the white contours) are densely packed in the islands, and each oligomer is formed by “single-leg” coupled H-motifs through Au adatoms. In particular, a long chain with multiple H-motifs is shown in Figure 3h. It is noteworthy that due to the separation of halogens in the form of NaX islands from molecular structures, the recovery of herringbone reconstructions of the Au(111) surface could be clearly observed from the large-scale STM images (Figure S6, 3e), verifying the cleanness of blank areas, which is distinct from the situation of the halogen-covered samples without the participation of Na.

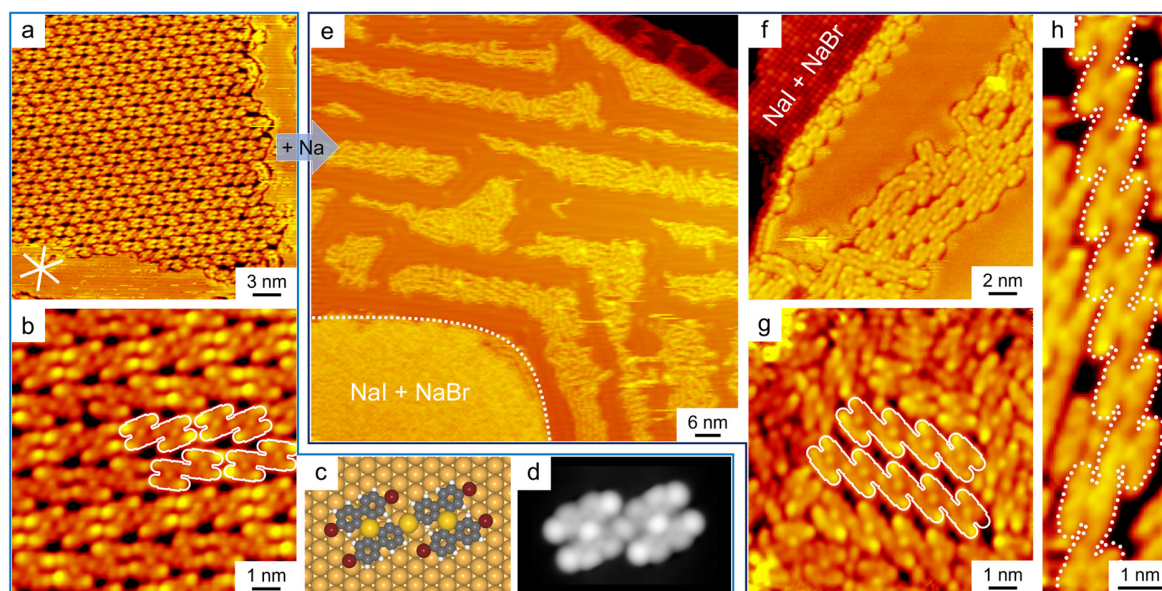


Figure 3. Further dehalogenative coupling with the formation of organometallic oligomers and NaX islands induced by Na at ~300 K. (a) Large-scale and (b) close-up STM images showing the formation of molecular islands composed of H-based organometallic dimers as typically depicted by the white contours. (c) DFT-optimized model and (d) simulated STM image of an H-motif on Au(111). C: gray; H: white; Br: brown; Au: yellow. (e) Large-scale and (f) close-up STM images showing the coexistence of molecular islands consisting of H-based

1
2
3
4
5
6 organometallic oligomers and isolated NaX islands. (g) Magnified STM image showing more
7
8 details of H-based organometallic oligomers (depicted by the white contours). (h) High-resolution
9
10 STM image of an individual H-based chain highlighted in the white contour. The close-packed
11
12 directions are indicated in (a). Scanning conditions: $V = -1.2$ V, $I = 0.5$ nA, and $T = 100 - 150$ K.
13
14

15
16 Furthermore, to experimentally discriminate the role of Na in the reaction process, a Na-free
17
18 control experiment was carried out (Figure S7). After annealing the sample precovered with H-
19
20 motifs at ~ 360 K, no change was observed (Figure S7a). Only when the annealing temperature
21
22 reached ~ 390 K did organometallic dimers form, surrounded by dissociated halogens (Figure S7b).
23
24 Further increase of the annealing temperature to ~ 410 K resulted in the construction of
25
26 organometallic oligomers, unfortunately accompanied by the desorption of most of the molecules
27
28 (Figure S7c). Consequently, it is concluded that the presence of Na promoted the dehalogenative
29
30 coupling of H-motifs without affecting the product structures and, more importantly, contributed
31
32 to the separation of halogens from molecular structures.
33
34

35
36 In an attempt to explore the universality of the role of Na in the dehalogenative reactions, a
37
38 simplified molecule, DBTP (cf. Figure 4a), which has only one type of functional group ($C_{\text{aryl}}\text{-Br}$)
39
40 as a typical Ullmann-type precursor and, more importantly, has been extensively reported with a
41
42 rich database for direct comparison with our experiments, was selected as a more general
43
44 molecular precursor for the model system. After deposition of DBTP on Au(111) held at ~ 300 K,
45
46 large molecular islands were observed (Figure 4b), consisting of intact DBTP molecules (depicted
47
48 by white rod-shaped contours and superimposed with structural models as shown in Figure 4c).
49
50 Meanwhile, residual Br atoms (depicted by blue circles), which were deliberately introduced to
51
52 verify the feasibility of separating free halogen atoms from this molecular system, were found to
53
54 coexist at a DBTP/Br stoichiometric ratio of $\sim 1:2$, providing the opportunity to demonstrate the
55
56
57
58
59
60

1
2
3
4
5
6 role of extrinsic Na in the isolation of intermolecular halogens in a more general case. Also note
7
8 that without the introduction of residual Br atoms, two kinds of self-assembled molecular
9
10 structures were obtained after deposition of pure DBTP molecules onto Au(111) (see Figure S8
11
12 and detailed discussions in the supporting information). Accordingly, Na was gradually dosed to
13
14 such a “DBTP + Br” sample kept at ~300 K, and separation of pure DBTP islands with a crossed
15
16 self-assembled arrangement (which is identical to that of pure DBTP molecules upon deposition,
17
18 see Figure S8) and salt (NaBr) islands was achieved (Figure 4d). From the close-up STM image
19
20 (Figure 4e), it is unambiguously seen that Br atoms were thoroughly separated from DBTP islands,
21
22 resulting in the obvious structural transformation, while the morphology of individual molecules
23
24 remained the same. Hence, the Na-induced separation strategy for intermolecular halogens was
25
26 generally validated as effective. Subsequently, more Na atoms were dosed and the sample was
27
28 annealed at ~340 K for ~10 h, and interestingly, two distinct separate structures could be identified
29
30 (with the boundary represented by the white dotted line), coexisting with NaBr islands (Figure 4f).
31
32 A large number of islands composed of longer molecular rods appeared, while halogen-free
33
34 crossed DBTP islands remained the same (see the upper right island). The magnified STM image
35
36 (Figure 4g) further shows that the newly generated close-packed molecular structures are attributed
37
38 to the DBTP-based oligomers, dominantly C–C coupled dimers and trimers (as depicted by the
39
40 light and dark green contours and overlaid with the corresponding structural models, respectively),
41
42 indicating the occurrence of dehalogenative coupling at quite low temperatures (ca. ~340 K) on
43
44 Au(111) in the presence of Na atoms in a general case.
45
46
47
48
49
50
51
52
53
54
55
56
57
58
59
60

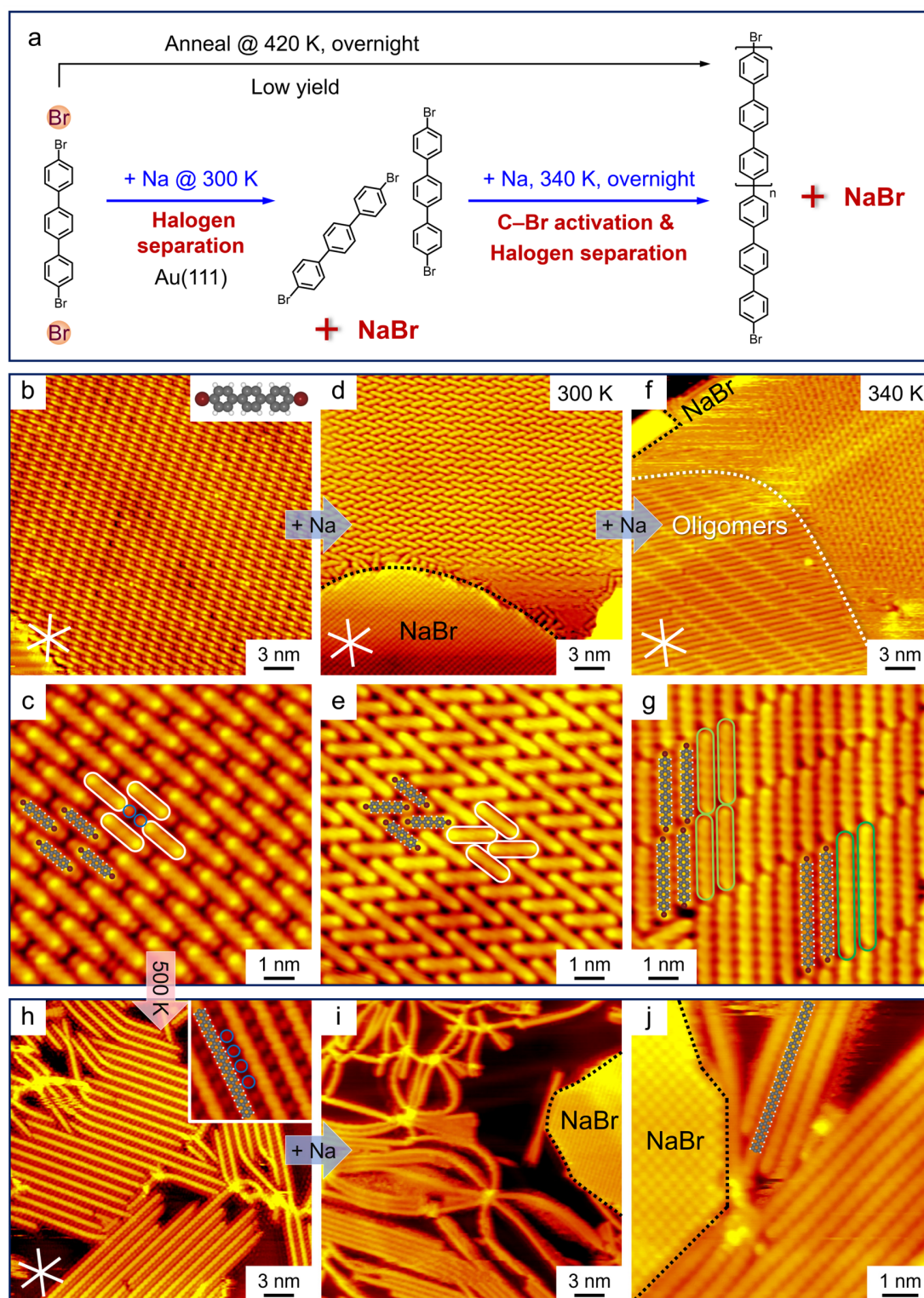


Figure 4. Na-induced halogen separation in the DBTP system on Au(111). (a) Schematic illustration showing the Na-facilitated halogen separation process and the Na-free process

1
2
3
4
5
6 indicated by blue and black arrows, respectively. (b, d) Large-scale and (c, e) close-up STM images
7
8 showing the structural transformation from (b, c) DBTP self-assembled structures coexisting with
9
10 residual Br atoms to (d, e) pure DBTP islands and NaBr islands (separated by the black dotted line)
11
12 after progressive Na deposition at ~ 300 K. Inset of (b): the structural model of DBTP. The
13
14 individual DBTP molecules are typically depicted by white rod-shaped contours and superimposed
15
16 with models, and Br atoms are indicated by blue circles. (f) Large-scale and (g) close-up STM
17
18 images showing the formation of molecular islands composed of DBTP-based oligomers, with
19
20 remaining DBTP molecules and NaBr islands after further deposition of Na and annealing at ~ 340
21
22 K for ~ 10 h. (h) Large-scale STM image showing the formation of long polyphenylene chains with
23
24 dissociated inter-chain Br atoms after annealing the DBTP-precovered sample at ~ 500 K for 10
25
26 min. Inset: magnified STM image (size: $4 \text{ nm} \times 4 \text{ nm}$) overlaid with the structural model of a
27
28 polyphenylene chain. (i) Large-scale and (j) close-up STM images showing the separation of
29
30 polyphenylene chains and NaBr islands (with the boundaries highlighted in black dotted lines)
31
32 after dosing Na at ~ 300 K. The close-packed directions are indicated in white lines. Scanning
33
34 conditions: $V = -1.2 \text{ V}$, $I = 0.5 \text{ nA}$, and $T = 100 - 150 \text{ K}$.
35
36
37
38
39

40 Notably, a Na-free control experiment was also conducted, where no change was observed under
41
42 the same condition, and after further annealing the DBTP-precovered Au(111) sample at ~ 420 K
43
44 for ~ 10 h, only a small number of dimers appeared that co-assembled with intact ones and were
45
46 separated by inter-row Br atoms (Figure S9), distinct from the Na-involved situation. In addition,
47
48 long polyphenylene chains with numerous Br atoms coexisting between the chains (highlighted by
49
50 blue circles in the inset) were obtained only after annealing such a sample at ~ 500 K for 10 min
51
52 (Figure 4h). A similar trick was played again by dosing Na to the sample at ~ 300 K, and the
53
54 polyphenylene chains turned to be tightly packed with a decreased inter-chain distance, while
55
56
57
58
59
60

1
2
3
4
5
6 NaBr salt islands were generated away from the molecular structures (Figure 4i, j), further
7
8 verifying the feasibility of the intermolecular halogen separation even from long chains. Note that
9
10 to further provide experimental evidence for the formation and assignment of NaI and NaBr islands
11
12 after deposition of pure Na atoms onto the corresponding dehalogenative systems on Au(111) (via
13
14 the separation of dissociated halogen atoms), we have directly deposited the corresponding salts
15
16 (NaI and NaBr) on Au(111) and compared their differences in morphologies and periodicities
17
18 (Figure S10), which are found to be in good agreement with each other and with the reported
19
20 values. Therefore, the halogen separation strategy by introducing extrinsic sodium onto Au(111)
21
22 has been demonstrated in general cases.
23
24
25

26 To further reveal the role of Na, the debromination pathways of both the H-motif and the DBTP
27
28 molecule were calculated using the DFT-based transition-state search as shown in Figure 5. For
29
30 the H-motif adsorbed on Au(111), one “leg” of each side is closer to the substrate due to the steric
31
32 hindrance, as can be seen from the side view of the initial state (IS) in Figure 5a, resulting in easier
33
34 debromination⁴² and consequently formation of “single-leg” coupled products. In the absence of
35
36 Na, the energy barrier of debromination was calculated to be ~ 1.21 eV, and the debrominated
37
38 product (FS) was energetically less stable than the IS by ~ 0.37 eV, indicating that the
39
40 debromination is an endothermic process. Upon the introduction of Na (cf. the bottom row in
41
42 Figure 5a), IS+Na (H-motif) with the Na atom isolated is energetically less favorable (0.36 eV
43
44 with respect to IS_Na), until the Na meets with the H-motif and stays in between two Br
45
46 substituents (IS_Na, 0 eV) via electrostatic interactions^{37, 38}, which is also consistent with the
47
48 interactions within the honeycomb structures. With the assistance of Na, the Br atom from the H-
49
50 motif is attracted to the Na atom (TS_Na) and then thoroughly bonded to it, and meanwhile, the
51
52 debrominated H-motif-based radical directly interacts with the underlying substrate in a bent-down
53
54
55
56
57
58
59
60

1
2
3
4
5
6 configuration, similar to the situation of the Na-free FS. Consequently, the Na-supported
7
8 debromination barrier was reduced to 1.00 eV. In addition, the FS_Na (H-motif) was calculated to
9
10 be more stable than IS+Na (H-motif), yet less stable than IS_Na (H-motif) by ~ 0.19 eV. It is also
11
12 noteworthy that the coexistence of H-based organometallic oligomers or chains and NaX salt
13
14 islands was experimentally observed, indicating the diffusion and aggregation of NaX into islands
15
16 at RT. Accordingly, we believe that the energy released in the diffusion and aggregation process
17
18 of NaX into salt islands should be high enough to compensate for the energy deficit in the
19
20 dehalogenative reactions (obtained by the reaction-pathway calculations), while such an
21
22 exothermic formation process of salt islands could not be properly taken into account by DFT
23
24 calculations. More importantly, the combination of Na with halogens separated free halogen atoms
25
26 from the reaction systems, leading to the reaction equilibrium shift to the coupling side, especially
27
28 for the reversible Ullmann reaction on Au(111).⁴³ Therefore, the participation of Na atoms was
29
30 revealed to facilitate the reaction not only in reducing the reaction barrier, but also in regulating
31
32 the reaction equilibrium.
33
34
35

36
37 As an extension of a more general case, the debromination processes of the DBTP molecule both
38
39 with and without the Na atom were calculated and shown in Figure 5b. Similarly, the Na atom
40
41 promoted the debromination process by lowering the reaction barrier from ~ 1.30 eV to ~ 1.10 eV,
42
43 as well as by stabilizing the reaction product, confirming the universality of the halogen separation
44
45 scenario of Na atoms. Moreover, Au(111) surface is the nice balance among catalytic activity,
46
47 molecular mobility, and relatively weak adsorption energy for radicals in C–X activation. The Au–
48
49 Br and Au–C signals were observed in XPS experiments with the cleavage of C–Br bonds as a
50
51 function of annealing temperatures in several dehalogenative systems on Au(111)^{11, 43, 44},
52
53 indicating the important role of Au(111). At the same time, despite the crucial role of Au adatoms
54
55
56
57
58
59
60

1
2
3
4
5
6 in on-surface reactions,⁴⁵⁻⁴⁷ the exact role of Au adatoms is generally difficult to be experimentally
7
8 discriminated on Au(111)^{45, 46} as they are always available at or above RT. Thus, we believe that
9
10 the Au(111) substrate (including Au adatoms) should also play an important role in the whole
11
12 reaction processes. Nevertheless, with the presence of Au adatoms in all the cases shown above,
13
14 the introduction of Na atoms has been demonstrated to both isolate the dissociated halogens and
15
16 facilitate the C–Br activation under mild conditions compared to the Na-free cases, confirming it
17
18 to be the dominant effect.
19
20

21
22 Furthermore, considering the three following aspects: (1) the highly programmable
23
24 characteristics and wide applications of Ullmann-type dehalogenative coupling reactions in the
25
26 field of on-surface synthesis; (2) the fact that dissociated halogens chemisorbed on Au(111)
27
28 usually impede the diffusion of dehalogenated radicals via a reversible recombination^{11,43}, prohibit
29
30 the generation of longer polymers⁴⁴, and interfere with the property characterization^{30, 48, 49}; (3) the
31
32 difficulties in both eliminating dissociated halogens and reducing reaction barriers using the
33
34 previously reported strategies; it is of great value to develop an alternative strategy to overcome
35
36 these drawbacks and is thus significant for the atomically precise structural construction and
37
38 accurate property characterization.
39
40
41
42
43
44
45
46
47
48
49
50
51
52
53
54
55
56
57
58
59
60

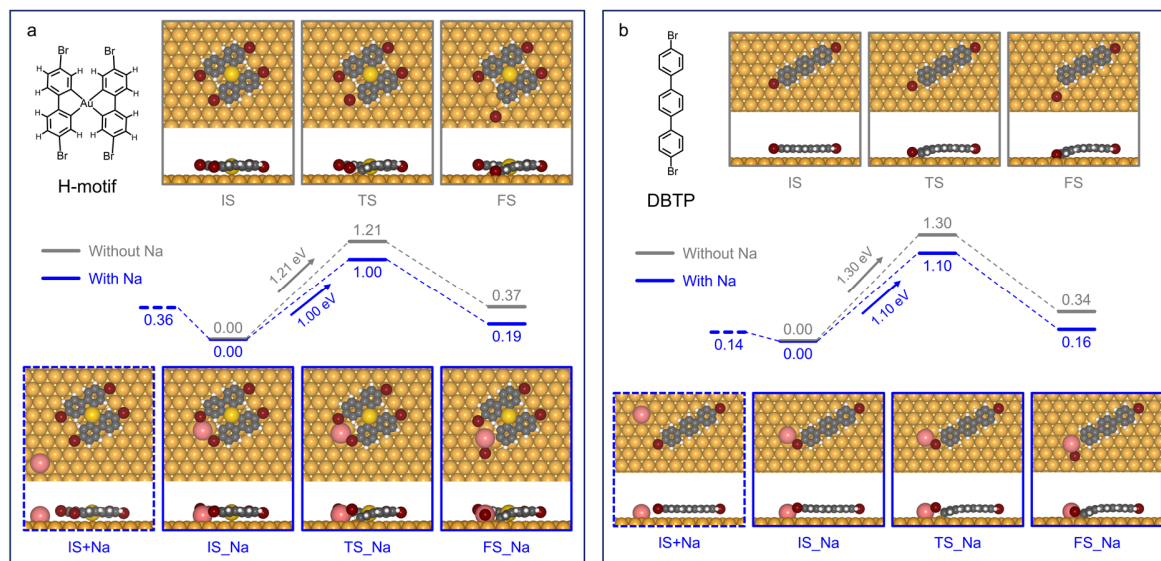


Figure 5. Reaction pathways for the C–Br activation of (a) H-motif and (b) DBTP molecule on Au(111) without (top panels) and with the assistance of Na (bottom panels), respectively. Structural models and energies of the initial states (IS), final states (FS), and transition states (TS) along the respective reaction pathways and the co-existence of the target molecule and Na without interaction (IS+Na) are given in the unit of eV with respect to the corresponding IS.

Conclusions

In conclusion, we have successfully developed a halogen separation strategy for dehalogenative reactions on Au(111) by introducing extrinsic Na atoms into molecular systems and demonstrated its versatility in both intermolecular halogen isolation and facilitation of intramolecular C–Br activation. Based on the model systems of the DBIBP molecule and the more general DBTP molecule, the combination of STM imaging and DFT calculations has experimentally and theoretically verified that this strategy is able to isolate free halogens by forming NaX islands and to promote the C–Br activation by lowering the reaction temperatures/barriers as well as by separating dissociated halogens from the reaction systems. Thus, the Na-induced C–Br activation

1
2
3
4
5
6 is feasible under mild conditions. Such an effective halogen separation strategy should be
7
8 promising in reducing the influence of halogen byproducts and significant for dehalogenation-
9
10 based programmed structure construction and accurate property characterization.
11
12

13 **Methods**

14
15
16
17 The STM experiments were performed in an ultrahigh vacuum (UHV) chamber with a base
18
19 pressure of 1×10^{-10} mbar equipped with a variable-temperature “Aarhus-type” STM from
20
21 SPECS^{50, 51}. The Au(111) substrate was cleaned by Ar⁺-ion sputtering and annealing at ~800 K for
22
23 repeated cycles. Two separate home-made molecular evaporators were used for the sample
24
25 preparation. After thorough degassing, the DBIBP and DBTP molecules (purchased from
26
27 Bidepharm and Adamas, with purity greater than 95% and 98%, respectively) were evaporated by
28
29 thermal sublimation at ~345 K and ~447 K, respectively, onto a clean Au(111) substrate held at
30
31 room temperature (RT, ~300 K). The pure sodium (Na, from SAES Getters) was dosed through
32
33 conventional resistance heating of a wire-type Na dispenser after complete degassing. The amount
34
35 of Na was calibrated and defined by applying a constant current (~6.5 A) for a time interval of 1.5
36
37 min once, and more Na was introduced by gradually increasing the number of deposition times.
38
39 The sodium halides (NaI and NaBr, purchased from Sigma-Aldrich, with purity greater than 99%)
40
41 were also evaporated by thermal sublimation. The sample was thereafter transferred within the
42
43 UHV chamber to the STM head for scanning. Typical scanning conditions: $V = -1.2$ V, and $I =$
44
45 $0.5 - 0.8$ nA. All the STM images were recorded in a typical temperature range of 100 – 150 K
46
47 and were further smoothed to eliminate noises.
48
49
50
51

52
53 The calculations were performed in the framework of DFT by using the Vienna ab initio simulation
54
55 package (VASP).^{52, 53} The projector-augmented wave method was used to describe the interaction
56
57
58
59
60

1
2
3
4
5
6 between ions and electrons.^{54, 55} The Perdew–Burke–Ernzerhof generalized gradient
7
8 approximation exchange–correlation functional was employed,⁵⁶ and van der Waals interactions
9
10 were included using the dispersion-corrected DFT-D3 method of Grimme.⁵⁷ The atomic structures
11
12 were relaxed using the conjugate gradient algorithm scheme as implemented in the VASP code
13
14 until the forces on all unconstrained atoms were ≤ 0.03 eV/Å. Plane waves were used as a basis
15
16 set with an energy cutoff of 400 eV. The simulated STM images were obtained by using the
17
18 Tersoff–Hamann method⁵⁸, in which the local density of states (LDOS) is used to approximate the
19
20 tunneling current. The Au(111) substrates were modeled by a three-layered slab separated by a
21
22 ~ 15 Å vacuum region for the structural models, where the bottom layer was fixed. Transition states
23
24 were searched by the climbing image nudged elastic band (CI-NEB)⁵⁹ and dimer methods⁶⁰, and
25
26 all the local minima and saddle points were optimized until the forces on all unconstrained atoms
27
28 were ≤ 0.03 eV/Å.
29
30
31
32
33
34
35
36

37 ASSOCIATED CONTENT

38 39 40 **Supporting Information.**

41
42
43 Supplementary STM images and DFT calculations (PDF).
44
45

46 AUTHOR INFORMATION

47 48 49 **Corresponding Author**

50
51 * E-mail:

52
53
54 Chi Zhang: zhangchi11@tongji.edu.cn;
55
56
57
58
59
60

1
2
3
4
5
6 Wei Xu: xuwei@tongji.edu.cn
7
8

9 **Author Contributions**

10
11 The manuscript was written through contributions of all authors. All authors have given approval
12 to the final version of the manuscript.
13
14
15

16 **Notes**

17
18
19 The authors declare no competing financial interest.
20
21

22 **ACKNOWLEDGMENT**

23
24 The authors acknowledge financial support from the Ministry of Science and Technology of the
25 People's Republic of China (2023YFE0101900), the National Natural Science Foundation of
26 China (Grants Nos. 22202153, 22125203, and 21790351), and the Fundamental Research Funds
27 for the Central Universities. The authors are grateful for the use of RIKEN's HOKUSAI
28 supercomputer system. The authors are also grateful for the fruitful discussion with Dr. Yuanqi
29 Ding.
30
31
32
33
34
35
36
37
38

39 **REFERENCES**

- 40
41 (1) Grill, L.; Hecht, S. Covalent On-Surface Polymerization. *Nat. Chem.* **2020**, *12*, 115-130.
42
43
44 (2) Talirz, L.; Ruffieux, P.; Fasel, R. On-Surface Synthesis of Atomically Precise Graphene
45 Nanoribbons. *Adv. Mater.* **2016**, *28*, 6222-6231.
46
47
48
49 (3) Clair, S.; de Oteyza, D. G. Controlling a Chemical Coupling Reaction on a Surface: Tools
50 and Strategies for On-Surface Synthesis. *Chem. Rev.* **2019**, *119*, 4717-4776.
51
52
53
54
55
56
57
58
59
60

- 1
2
3
4
5
6 (4) Fan, Q.; Gottfried, J. M.; Zhu, J. Surface-Catalyzed C–C Covalent Coupling Strategies
7
8 toward the Synthesis of Low-Dimensional Carbon-Based Nanostructures. *Acc. Chem. Res.* **2015**,
9
10 *48*, 2484-2494.
11
12
13 (5) Zhang, C.; Yi, Z.; Xu, W. Scanning Probe Microscopy in Probing Low-Dimensional Carbon-
14
15 Based Nanostructures and Nanomaterials. *Mater. Futures* **2022**, *1*, 032301.
16
17
18 (6) Grill, L.; Dyer, M.; Lafferentz, L.; Persson, M.; Peters, M. V.; Hecht, S. Nano-Architectures
19
20 by Covalent Assembly of Molecular Building Blocks. *Nat. Nanotechnol.* **2007**, *2*, 687-691.
21
22
23 (7) Cai, J.; Ruffieux, P.; Jaafar, R.; Bieri, M.; Braun, T.; Blankenburg, S.; Muoth, M.; Seitsonen,
24
25 A. P.; Saleh, M.; Feng, X.; et al. Atomically Precise Bottom-Up Fabrication of Graphene
26
27 Nanoribbons. *Nature* **2010**, *466*, 470-473.
28
29
30 (8) Fan, Q.; Martin-Jimenez, D.; Werner, S.; Ebeling, D.; Koehler, T.; Vollgraff, T.;
31
32 Sundermeyer, J.; Hieringer, W.; Schirmeisen, A.; Gottfried, J. M. On-Surface Synthesis and
33
34 Characterization of a Cycloarene: C108 Graphene Ring. *J. Am. Chem. Soc.* **2020**, *142*, 894-899.
35
36
37 (9) Zhang, C.; Kazuma, E.; Kim, Y. Atomic-Scale Visualization of the Stepwise Metal-Mediated
38
39 Dehalogenative Cycloaddition Reaction Pathways: Competition between Radicals and
40
41 Organometallic Intermediates. *Angew. Chem. Int. Ed.* **2019**, *58*, 17736-17744.
42
43
44 (10) Björk, J.; Hanke, F.; Stafström, S. Mechanisms of Halogen-Based Covalent Self-Assembly
45
46 on Metal Surfaces. *J. Am. Chem. Soc.* **2013**, *135*, 5768-5775.
47
48
49
50
51
52
53
54
55
56
57
58
59
60

- 1
2
3
4
5
6 (11) Batra, A.; Cvetko, D.; Kladnik, G.; Adak, O.; Cardoso, C.; Ferretti, A.; Prezzi, D.; Molinari,
7
8 E.; Morgante, A.; Venkataraman, L. Probing the Mechanism for Graphene Nanoribbon
9
10 Formation on Gold Surfaces through X-Ray Spectroscopy. *Chem. Sci.* **2014**, *5*, 4419-4423.
11
12
13 (12) Fritton, M.; Duncan, D. A.; Deimel, P. S.; Rastgoo-Lahrood, A.; Allegretti, F.; Barth, J. V.;
14
15 Heckl, W. M.; Björk, J.; Lackinger, M. The Role of Kinetics versus Thermodynamics in Surface-
16
17 Assisted Ullmann Coupling on Gold and Silver Surfaces. *J. Am. Chem. Soc.* **2019**, *141*, 4824-
18
19 4832.
20
21
22 (13) Abyazisani, M.; MacLeod, J. M.; Lipton-Duffin, J. Cleaning up after the Party: Removing
23
24 the Byproducts of On-Surface Ullmann Coupling. *ACS Nano* **2019**, *13*, 9270-9278.
25
26
27 (14) Zuzak, R.; Jančařík, A.; Gourdon, A.; Szymonski, M., Godlewski, S. On-Surface Synthesis
28
29 with Atomic Hydrogen. *ACS Nano* **2020**, *14*, 13316-13323.
30
31
32 (15) Sun, K.; Nishiuchi, T.; Sahara, K.; Kubo, T.; Foster, A. S.; Kawai, S. Low-Temperature
33
34 Removal of Dissociated Bromine by Silicon Atoms for an On-Surface Ullmann Reaction. *J.*
35
36 *Phys. Chem. C* **2020**, *124*, 19675-19680.
37
38
39 (16) Enderson, Z. A.; Murali, H.; Dasari, R. R.; Dai, Q.; Li, H.; Parker, T. C.; Brédas, J.-L.;
40
41 Marder, S. R.; First, P. N. Tailoring On-Surface Molecular Reactions and Assembly through
42
43 Hydrogen-Modified Synthesis: From Triarylamine Monomer to 2D Covalent Organic
44
45 Framework. *ACS Nano* **2023**, *17*, 7366-7376.
46
47
48 (17) Sun, K.; Silveira, O. J.; Ma, Y.; Hasegawa, Y.; Matsumoto, M.; Kera, S.; Krejčí, O.; Foster,
49
50 A. S.; Kawai, S. On-Surface Synthesis of Disilabenzene-Bridged Covalent Organic Frameworks.
51
52 *Nat. Chem.* **2022**, *15*, 136-142.
53
54
55
56
57
58
59
60

- 1
2
3
4
5
6 (18) Lin, T.; Shang, X. S.; Adisoejoso, J.; Liu, P. N.; Lin, N. Steering On-Surface
7
8 Polymerization with Metal-Directed Template. *J. Am. Chem. Soc.* **2013**, *135*, 3576-3582.
9
10
11 (19) Adisoejoso, J.; Lin, T.; Shang, X. S.; Shi, K. J.; Gupta, A.; Liu, P. N.; Lin, N. A Single-
12
13 Molecule-Level Mechanistic Study of Pd-Catalyzed and Cu-Catalyzed Homocoupling of Aryl
14
15 Bromide on an Au(111) Surface. *Chem. Eur. J.* **2014**, *20*, 4111-4116.
16
17
18 (20) Xing, S.; Liu, B.; Wang, W.; Guo, J.; Wang, W. On-Surface Synthesis of Graphene
19
20 Nanoribbons Catalyzed by Ni Atoms. *Chem. Asian J.* **2018**, *13*, 2023-2026.
21
22
23 (21) Cirera, B.; Björk, J.; Otero, R.; Gallego, J. M.; Miranda, R.; Ecija, D. Efficient Lanthanide
24
25 Catalyzed Debromination and Oligomeric Length-Controlled Ullmann Coupling of Aryl Halides.
26
27 *J. Phys. Chem. C* **2017**, *121*, 8033-8041.
28
29
30 (22) Feng, L.; Wang, T.; Jia, H.; Huang, J.; Han, D.; Zhang, W.; Ding, H.; Xu, Q.; Du, P.; Zhu, J.
31
32 On-Surface Synthesis of Planar Acenes via Regioselective Aryl-Aryl Coupling. *Chem. Commun.*
33
34 **2020**, *56*, 4890-4893.
35
36
37 (23) Zhang, H.; Franke, J. -H.; Zhong, D.; Li, Y.; Timmer, A.; Arado, O. D.; Mönig, H.; Wang,
38
39 H.; Chi, L.; Wang, Z.; et al. Surface Supported Gold-Organic Hybrids: On-Surface Synthesis and
40
41 Surface Directed Orientation. *Small* **2014**, *10*, 1361-1368.
42
43
44 (24) Liu, M.; Liu, M.; She, L.; Zha, Z.; Pan, J.; Li, S.; Li, T.; He, Y.; Cai, Z.; Wang, J.; et al.
45
46 Graphene-Like Nanoribbons Periodically Embedded with Four- and Eight-Membered Rings.
47
48 *Nat. Commun.* **2017**, *8*, 14924.
49
50
51
52
53
54
55
56
57
58
59
60

- 1
2
3
4
5
6 (25) Lafferentz, L.; Eberhardt, V.; Dri, C.; Africh, C.; Comelli, G.; Esch, F.; Hecht, S.; Grill, L.
7
8 Controlling On-Surface Polymerization by Hierarchical and Substrate-Directed Growth. *Nat.*
9
10 *Chem.* **2012**, *4*, 215-220.
11
12
13 (26) Zhong, Q.; Niu, K.; Chen, L.; Zhang, H.; Ebeling, D.; Björk, J.; Müllen, K.; Schirmeisen,
14
15 A.; Chi, L. Substrate-Modulated Synthesis of Metal-Organic Hybrids by Tunable Multiple Aryl-
16
17 Metal Bonds. *J. Am. Chem. Soc.* **2022**, *144*, 8214-8222.
18
19
20 (27) Gao, Y.; Zhang, Z.; Yi, Z.; Zhang, C.; Xu, W. Visualizing the Hierarchical Evolution of
21
22 Aryl–Metal Bonding in Organometallic Nanostructures on Ag(111). *J. Phys. Chem. Lett.* **2023**,
23
24 *14*, 10819-10824.
25
26
27 (28) Jang, W. J.; Chung, K.-H.; Lee, M. W.; Kim, H.; Lee, S.; Kahng, S.-J. Tetragonal Porous
28
29 Networks Made by Rod-Like Molecules on Au(111) with Halogen Bonds. *Appl. Surf. Sci.* **2014**,
30
31 *309*, 74-78.
32
33
34 (29) Shang, J.; Wang, Y.; Chen, M.; Dai, J.; Zhou, X.; Kuttner, J.; Hilt, G.; Shao, X.; Gottfried,
35
36 J. M.; Wu, K. Assembling Molecular Sierpiński Triangle Fractals. *Nat. Chem.* **2015**, *7*, 389-393.
37
38
39 (30) Kawai, S.; Takahashi, K.; Ito, S.; Pawlak, R.; Meier, T.; Spijker, P.; Canova, F. F.; Tracey,
40
41 J.; Nozaki, K.; Foster, A. S.; et al. Competing Annulene and Radialene Structures in a Single
42
43 Anti-Aromatic Molecule Studied by High-Resolution Atomic Force Microscopy. *ACS Nano*
44
45 **2017**, *11*, 8122-8130.
46
47
48 (31) Xie, L.; Zhang, C.; Ding, Y.; Xu, W. Structural Transformation and Stabilization of Metal-
49
50 Organic Motifs Induced by Halogen Doping. *Angew. Chem. Int. Ed.* **2017**, *56*, 5077-5081.
51
52
53
54
55
56
57
58
59
60

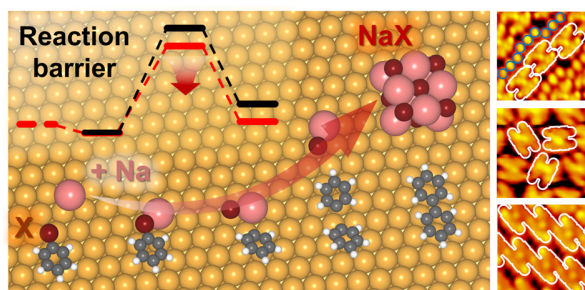
- 1
2
3
4
5
6 (32) Jiménez-Martín, A.; Gallardo, A.; de la Torre, B. Coverage-Modulated Halogen Bond
7
8 Geometry Transformation in Supramolecular Assemblies. *Nanoscale* **2023**, *15*, 16354-16361.
9
10
11 (33) Hou, R.; Guo, Y.; Yi, Z.; Zhang, Z.; Zhang, C.; Xu, W. Construction and Structural
12
13 Transformation of Metal–Organic Nanostructures Induced by Alkali Metals and Alkali Metal
14
15 Salts. *J. Phys. Chem. Lett.* **2023**, *14*, 3636-3642.
16
17
18 (34) Lin, Y.; Huang, Z.; Wen, X.; Rong, W.; Peng, Z.; Diao, M.; Xing, L.; Dai, J.; Zhou, X.; Wu,
19
20 K. Steering Effect of Bromine on Intermolecular Dehydrogenation Coupling of Poly(p-
21
22 phenylene) on Cu(111). *ACS Nano* **2020**, *14*, 17134-17141.
23
24
25
26 (35) Yi, Z.; Zhang, C.; Zhang, Z.; Hou, R.; Guo, Y.; Xu, W. On-Surface Synthesis of Na-
27
28 Porphyrins Using NaCl as a Convenient Na Source. *Precis. Chem.* **2023**, *1*, 226-232.
29
30
31
32 (36) Yi, Z.; Guo, Y.; Hou, R.; Zhang, Z.; Gao, Y.; Zhang, C.; Xu, W. Revealing the Orientation
33
34 Selectivity of Tetrapyrrolyl-Substituted Porphyrins Constrained in Molecular “Klotski Puzzles”.
35
36 *J. Am. Chem. Soc.* **2023**, *145*, 22366-22373.
37
38
39
40 (37) Dai, J.; Zhao, X.; Peng, Z.; Li, J.; Lin, Y.; Wen, X.; Xing, L.; Zhao, W.; Shang, J.; Wang,
41
42 Y.; et al. Assembling Surface Molecular Sierpiński Triangle Fractals via K⁺-Invoked
43
44 Electrostatic Interaction. *J. Am. Chem. Soc.* **2023**, *145*, 13531-13536.
45
46
47
48 (38) Shan, H.; Zhou, L.; Ji, W.; Zhao, A. Flexible Alkali–Halogen Bonding in Two Dimensional
49
50 Alkali-Metal Organic Frameworks. *J. Phys. Chem. Lett.* **2021**, *12*, 10808-10814.
51
52
53
54
55
56
57
58
59
60

- 1
2
3
4
5
6 (39) Berdonces-Layunta, A.; Schulz, F.; Aguilar-Galindo, F.; Lawrence, J.; Mohammed, M. S.
7
8 G.; Muntwiler, M.; Lobo-Checa, J.; Liljeroth, P.; de Oteyza, D. G. Order from a Mess: The
9
10 Growth of 5-Armchair Graphene Nanoribbons. *ACS Nano* **2021**, *15*, 16552-16561.
11
12
13 (40) Galeotti, G.; De Marchi, F.; Taerum, T.; Besteiro, L. V.; El Garah, M.; Lipton-Duffin, J.;
14
15 Ebrahimi, M.; Perepichka, D. F.; Rosei, F. Surface-Mediated Assembly, Polymerization and
16
17 Degradation of Thiophene-Based Monomers. *Chem. Sci.* **2019**, *10*, 5167-5175.
18
19
20 (41) Qin, T.; Guo, D.; Xiong, J.; Li, X.; Hu, L.; Yang, W.; Chen, Z.; Wu, Y.; Ding, H.; Hu, J.; et
21
22 al. Synthesis of a Porous [14]Annulene Graphene Nanoribbon and a Porous [30]Annulene
23
24 Graphene Nanosheet on Metal Surfaces. *Angew. Chem. Int. Ed.* **2023**, e202306368.
25
26
27 (42) Merino-Díez, N.; Pérez Paz, A.; Li, J.; Vilas-Varela, M.; Lawrence, J.; Mohammed, M. S.
28
29 G.; Berdonces-Layunta, A.; Barragán, A.; Pascual, J. I.; Lobo-Checa, J.; et al. Hierarchy in the
30
31 Halogen Activation During Surface-Promoted Ullmann Coupling. *ChemPhysChem* **2019**, *20*,
32
33 2305-2310.
34
35
36 (43) Stolz, S.; Di Giovannantonio, M.; Urgel, J. I.; Sun, Q.; Kinikar, A.; Borin Barin, G.;
37
38 Bommert, M.; Fasel, R.; Widmer, R. Reversible Dehalogenation in On-Surface Aryl-Aryl
39
40 Coupling. *Angew. Chem. Int. Ed.* **2020**, *59*, 14106-14110.
41
42
43 (44) Di Giovannantonio, M.; Deniz, O.; Urgel, J. I.; Widmer, R.; Dienel, T.; Stolz, S.; Sánchez-
44
45 Sánchez, C.; Muntwiler, M.; Dumsloff, T.; Berger, R., et al. On-Surface Growth Dynamics of
46
47 Graphene Nanoribbons: The Role of Halogen Functionalization. *ACS Nano* **2018**, *12*, 74-81.
48
49
50
51
52
53
54
55
56
57
58
59
60

- 1
2
3
4
5
6 (45) Lowe, B.; Hellerstedt, J.; Matěj, A.; Mutombo, P.; Kumar, D.; Ondráček, M.; Jelinek, P.;
7
8 Schiffrin, A. Selective Activation of Aromatic C–H Bonds Catalyzed by Single Gold Atoms at
9
10 Room Temperature. *J. Am. Chem. Soc.* **2022**, *144*, 21389–21397.
11
12
13 (46) Björk, J.; Sánchez-Sánchez, C.; Chen, Q.; Pignedoli, C. A.; Rosen, J.; Ruffieux, P.; Feng,
14
15 X.; Narita, A.; Müllen, K.; Fasel, R. The Role of Metal Adatoms in a Surface-Assisted
16
17 Cyclodehydrogenation Reaction on a Gold Surface. *Angew. Chem. Int. Ed.* **2022**, *61*,
18
19 e202212354.
20
21
22
23 (47) Zhang, Z.; Perepichka, D. F.; Khaliullin, R. Z. Adatoms in the Surface-Confined Ullmann
24
25 Coupling of Phenyl Groups. *J. Phys. Chem. Lett.* **2021**, *12*, 11061–11069.
26
27
28 (48) Rastgoo-Lahrood, A.; Lischka, M.; Eichhorn, J.; Samanta, D.; Schmittel, M.; Heckl, W. M.;
29
30 Lackinger, M. Reversible Intercalation of Iodine Monolayers between On-Surface Synthesised
31
32 Covalent Polyphenylene Networks and Au(111). *Nanoscale* **2017**, *9*, 4995–5001.
33
34
35
36 (49) Rastgoo-Lahrood, A.; Björk, J.; Lischka, M.; Eichhorn, J.; Kloft, S.; Fritton, M.; Strunskus,
37
38 T.; Samanta, D.; Schmittel, M.; Heckl, W. M.; et al. Post-Synthetic Decoupling of On-Surface-
39
40 Synthesized Covalent Nanostructures from Ag(111). *Angew. Chem. Int. Ed.* **2016**, *55*, 7650–
41
42 7654.
43
44
45
46 (50) Besenbacher, F. Scanning Tunnelling Microscopy Studies of Metal Surfaces. *Rep. Prog.*
47
48 *Phys.* **1996**, *59*, 1737–1802.
49
50
51
52 (51) Laegsgaard, E.; Österlund, L.; Thostrup, P.; Rasmussen, P. B.; Stensgaard, I.; Besenbacher,
53
54 F. A High-Pressure Scanning Tunneling Microscope. *Rev. Sci. Instrum.* **2001**, *72*, 3537–3542.
55
56
57
58
59
60

- 1
2
3
4
5
6 (52) Kresse, G.; Hafner, J. *Ab Initio* Molecular Dynamics for Open-Shell Transition
7
8 Metals. *Phys. Rev. B* **1993**, *48*, 13115–13118.
9
10
11 (53) Kresse, G.; Furthmüller, J. Efficient Iterative Schemes for *Ab Initio* Total-Energy
12
13 Calculations Using a Plane-Wave Basis Set. *Phys. Rev. B* **1996**, *54*, 11169–11186.
14
15
16 (54) Blöchl, P. E. Projector Augmented-Wave Method. *Phys. Rev. B* **1994**, *50*, 17953–17979.
17
18
19
20 (55) Kresse, G.; Joubert, D. From Ultrasoft Pseudopotentials to the Projector Augmented-Wave
21
22 Method. *Phys. Rev. B* **1999**, *59*, 1758–1775.
23
24
25 (56) Perdew, J. P.; Burke, K.; Ernzerhof, M. Generalized Gradient Approximation Made
26
27 Simple. *Phys. Rev. Lett.* **1996**, *77*, 3865–3868.
28
29
30
31 (57) Grimme, S.; Antony, J.; Ehrlich, S.; Krieg, H. A Consistent and Accurate *Ab*
32
33 *Initio* Parametrization of Density Functional Dispersion Correction (DFT-D) for the 94 Elements
34
35 H-Pu. *J. Chem. Phys.* **2010**, *132*, 154104.
36
37
38 (58) Tersoff, J.; Hamann, D. R. Theory of the Scanning Tunneling Microscope. *Phys. Rev. B*
39
40 **1985**, *31*, 805–813.
41
42
43 (59) Henkelman, G.; Uberuaga, B. P.; Jónsson, H. A Climbing Image Nudged Elastic Band
44
45 Method for Finding Saddle Points and Minimum Energy Paths. *J. Chem. Phys.* **2000**, *113*, 9901–
46
47 9904.
48
49
50
51 (60) Kästner, J.; Sherwood, P. Superlinearly Converging Dimer Method for Transition State
52
53 Search. *J. Chem. Phys.* **2008**, *128*, 014106.
54
55
56
57
58
59
60

1
2
3
4
5
6 TOC graphic
7
8
9



20
21 By the combination of scanning tunneling microscopy imaging and density functional theory
22 calculations, a versatile halogen separation strategy has been developed by introducing extrinsic
23 sodium (Na) into dehalogenative reactions on Au(111) as model systems that both isolates the
24 dissociated halogens and facilitates the C–Br activation under mild conditions.
25
26
27
28
29
30
31
32
33
34
35
36
37
38
39
40
41
42
43
44
45
46
47
48
49
50
51
52
53
54
55
56
57
58
59
60